DOI: 10.17344/acsi.2023.8370 *Acta Chim. Slov.* **2023,** *70,* 524–532

Scientific paper

Syntheses, Characterization, Crystal Structures and Xanthine Oxidase Inhibitory Activity of Hydrazones

Xiao-Jun Zhao, Ling-Wei Xue* and Qiao-Ru Liu

School of Chemical and Environmental Engineering, Pingdingshan University, Pingdingshan Henan 467000, P.R. China

** Corresponding author: E-mail: pdsuchemistry@163.com*

Received: 08-06-2023

Abstract

Four new fluoro-containing hydrazones were synthesized from 4-fluorobenzaldehyde with chloro- and nitro-substituted benzohydrazides. They are 3-chloro-*N*'-(4-fluorobenzylidene)benzohydrazide (**1**), 2-chloro-*N*'-(4-fluorobenzylidene) benzohydrazide (**2**), *N*'-(4-fluorobenzylidene)-4-nitrobenzohydrazide (**3**), and *N*'-(4-fluorobenzylidene)-3-nitrobenzohydrazide (**4**). The compounds have been characterized by IR and ^{1}H NMR spectroscopy, as well as X-ray single crystal determination. Xanthine oxidase (XO) inhibitory activity indicated that the nitro substituted compounds **3** and **4** have effective activity. Docking simulation was performed to insert the compounds into the crystal structure of xanthine oxidase at the active site to investigate the probable binding modes.

Keywords: Hydrazone; xanthine oxidase; inhibition; crystal structure; molecular docking study.

1. Introduction

Xanthine oxidase (XO; Enzyme Code 1.17.3.2) is a molybdenum hydroxylase, which catalyzes hypoxanthine and xanthine to form superoxide anions and uric acid. The superoxide anions are responsible for post ischaemic tissue injury and vascular permeability.[1] Xanthine oxidase has many negative effects. It can oxidize the purine drug antileukaemic 6-mercaptopurine to lose its pharmacological activity. Moreover, it can leads to hepatic and kidney damage, atherosclerosis, chronic heart failure, hypertension and sickle-cell disease.[2] Thus, it is necessary to control the activity of xanthine oxidase. Allopurinol is a well known XO inhibitor, which has been used as medicine to treat the gout.[3] However, it has obvious side effects like toxicity, and inability to prevent the formation of free radicals by the enzyme.[4] So, it is urgent to explore new xanthine oxidase inhibitors. To date, a large number of compounds like pyrimidines and carboxylic acids,[5] 3-cyanoindoles and pyrimidinones,[6] hydrozingerones,[7] amides,[8] pyrazoles,[9] thiobarbiturates,[10] have been reported to have xanthine oxidase inhibitory activity. Schiff bases with C=N functional group have received much attention in the fields of biological chemistry.[11] Leigh has reported a few Schiff bases with

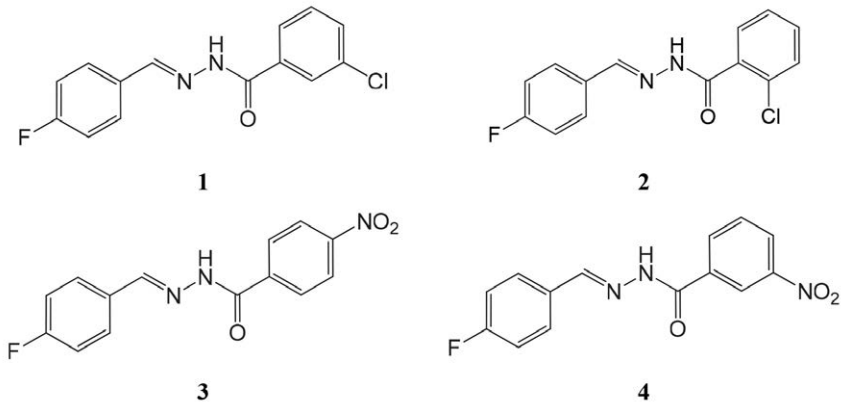

Scheme 1. The hydrazone compounds.

potential xanthine oxidase inhibitory activity.[12] Hydrazones are a special kind of Schiff base which possess the functional group C=N-NH-C(O). These compounds have interesting biological activities.[13] Moreover, the electronic withdrawing groups like F, Cl and NO_2 can improve the biological activities.[14] Recently, we have reported a series of hydrazones, and found that *N*'-(3-methoxybenzylidene)-4-nitrobenzohydrazide and 2-cyano-*N*'-(4-diethylamino-2-hydroxybenzylidene)acetohydrazide have effective activity on xanthine oxidase.[15] However, the xanthine oxidase inhibition of hydrazones has rarely been studied so far. Aiming at obtaining new xanthine oxidase inhibitors, we report herein four new hydrazones (Scheme 1), 3-chloro-*N*'-(4-fluorobenzylidene)benzohydrazide (**1**), 2-chloro-*N*'-(4-fluorobenzylidene)benzohydrazide (**2**), *N*'-(4-fluorobenzylidene)-4-nitrobenzohydrazide (**3**), and *N*'-(4-fluorobenzylidene)-3-nitrobenzohydrazide (**4**). were synthesized and characterized. Their xanthine oxidase inhibitory activity was studied.

2. Experimental

2. 1. Materials and Methods

4-Fluorobenzaldehyde, 3-chlorobenzohydrazide, 2-chlorobenzohydrazide, 4-nitrobenzohydrazide, 3-nitrobenzohydrazide and solvents were obtained from commercial suppliers and used as received. Elemental analyses for C, H and N were performed on a Perkin-Elmer 240C elemental analyzer. IR spectra were recorded on a Jasco FT/IR-4000 spectrometer as KBr pellets in the 4000–400 cm^{-1} region. ^1H NMR data were performed on a Bruker 300 MHz instrument. X-ray single crystal diffraction was determined on a Bruker SMART 1000 CCD diffractometer.

2. 2. Synthesis of the Compounds

The four compounds were synthesized with the same method as described. 4-Fluorobenzaldehyde (0.12 g, 1.0 mmol) and 1.0 mmol benzohydrazide were respectively dissolved in 20 mL methanol. Then, the two precursors were mixed and stirred at room temperature for 30 min to give clear solution. The solution was stand still in air, and slow evaporate for a few days to obtain X-ray quality single crystals.

3-Chloro-*N*'-(4-fluorobenzylidene)benzohydrazide (1)

The benzohydrazide is 3-chlorobenzohydrazide (0.17 g). Block colorless single crystals. Yield: 0.26 g (93%). Anal. Calc. for $C_{14}H_{12}ClFN_2O_2$ (%): C, 57.06; H, 4.10; N, 9.51. Found (%): C, 57.23; H, 3.97; N, 9.40. IR data (cm^{-1}): 3217w (NH), 1665s (C=O), 1600m (C=N). ^1H NMR (300 MHz, d_6-DMSO): δ 11.96 (s, 1H, N*H*), 8.46 (s, 1H, C*H*=N), 7.97 (s, 1H, Ar*H*), 7.88 (d, 1H, Ar*H*), 7.82 (d, 2H, Ar*H*), 7.70 (d, 1H, Ar*H*), 7.60 (t, 1H, Ar*H*), 7.32 (t, 2H, Ar*H*).

2-chloro-*N*'-(4-fluorobenzylidene)benzohydrazide (2)

The benzohydrazide is 2-chlorobenzohydrazide (0.17 g). Block colorless single crystals. Yield: 2.4 g (87%). Anal. Calc. for $C_{14}H_{10}ClFN_2O$ (%): C, 60.77; H, 3.64; N, 10.12. Found (%): C, 60.61; H, 3.72; N, 10.21. IR data (cm^{-1}): 3235w (NH), 1666s (C=O), 1602m (C=N). ^1H NMR (300 MHz, d_6-DMSO): δ 11.90 (s, 1H, N*H*), 8.28 (s, 1H, C*H*=N), 7.82 (d, 2H, Ar*H*), 7.55-7.60 (m, 2H, Ar*H*), 7.50 (m, 2H, Ar*H*), 7.30 (d, 1H, Ar*H*), 7.17 (t, 1H, Ar*H*).

***N*'-(4-fluorobenzylidene)-4-nitrobenzohydrazide (3)**

The benzohydrazide is 4-nitrobenzohydrazide (0.18 g). Prism yellow single crystals. Yield: 2.6 g (91%). Anal. Calc. for $C_{14}H_{10}FN_3O_3$ (%): C, 58.54; H, 3.51; N, 14.63. Found (%): C, 58.37; H, 3.62; N, 14.47. IR data (cm^{-1}): 3226w (NH), 1653s (C=O), 1604m (C=N), 1522s and 1345s (NO_2). ^1H NMR (300 MHz, d_6-DMSO): δ 12.17 (s, 1H, N*H*), 8.49 (s, 1H, C*H*=N), 8.40 (d, 2H, Ar*H*), 8.18 (d, 2H, Ar*H*), 7.85 (d, 2H, Ar*H*), 7.35 (d, 2H, Ar*H*).

***N*'-(4-fluorobenzylidene)-3-nitrobenzohydrazide (4)**

The benzohydrazide is 4-nitrobenzohydrazide (0.18 g). Block yellow single crystals. Yield: 2.5 g (87%). Anal. Calc. for $C_{14}H_{10}FN_3O_3$ (%): C, 58.54; H, 3.51; N, 14.63. Found (%): C, 58.41; H, 3.45; N, 14.50. IR data (cm^{-1}): 3227w (NH), 1649s (C=O), 1608m (C=N), 1532s and 1350s (NO_2). ^1H NMR (300 MHz, d_6-DMSO): δ 12.20 (s, 1H, N*H*), 8.78 (s, 1H, Ar*H*), 8.51 (s, 1H, C*H*=N), 8.48 (d, 1H, Ar*H*), 8.38 (d, 1H, Ar*H*), 7.89–7.82 (m, 3H, Ar*H*), 7.35 (d, 2H, Ar*H*).

2. 3. Xanthine Oxidase Inhibition Assay

The xanthine oxidase activity with xanthine as substrate was measured according to the method reported by Kong and co-workers with modification.[16] The activity of xanthine oxidase was measured by uric acid formation monitored at 295 nm. The assay was performed in K_2HPO_4 (1.0 mL, 50 mmol L^{-1}) in a quartz cuvette. The reaction mixture contains xanthine (200 μL, 84.8 μg mL^{-1}) in the solution of K_2HPO_4, and various concentrations of tested compounds (50 μL). The reaction was started by addition of xanthine oxidase (66 μL, 37.7 mU mL^{-1}), and monitored for 6 min at 295 nm and the product was expressed as μmol uric acid per minute. The reactions kinetic were linear during these 6 min of monitoring.

2. 4. Docking Simulations

Molecular docking study of the molecules of the hydrazones into the three-dimensional structure of xanthine oxidase (1FIQ in the Protein Data Bank) was carried out by using AutoDock 4.2. AutoGrid component of the program calculates a three-dimensional grid of interaction energies based on the macromolecular target using AMBER force field. The cubic grid box of 60 × 60 × 60 $Å^3$

points in *x*, *y*, and *z* direction with a spacing of 0.375 Å and grid maps were created representing the catalytic active target site region where the native ligand was embedded. Then automated docking studies were carried out to evaluate the biding free energy of the inhibitor within the macromolecules. The GALS search algorithm (genetic algorithm with local search) was chosen to search for the best conformers. The parameters were set using ADT (AutoDockTools 1.5.4) on PC which is associated with AutoDock 4.2. Default settings were used with an initial population of 100 randomly placed individuals, a maximum number of 2.5×10^6 energy evaluations, and a maximum number of 2.7×10^4 generations. A mutation rate of 0.02 and a crossover rate of 0.8 were chosen. Give overall consideration of the most favorable free energy of biding and the majority cluster, the results were selected as the most probable complex structures.

2. 5. Data Collection, Structural Determination and Refinement

The collected data were reduced with SAINT,[17] and multi-scan absorption correction was performed with SADABS.[18] The structures of the compounds were solved by direct method and refined against F^2 by full-matrix least-squares method using SHELXTL.[19] All non-hydrogen atoms were refined anisotropically. The water H atoms in **1**, and all amino H atoms in the four compounds were located from difference Fourier maps and refined isotropically, with O–H, N–H and H···H distances restrained to 0.85(1), 0.90(1) and 1.37(2) Å, respectively. The remaining H atoms were placed in calculated positions and constrained to ride on their parent atoms. The crystallographic data for the compounds are summarized in Table 1.

3. Results and Discussion

3. 1. Chemistry

The hydrazones were facile prepared by reaction of 4-fluorobenzaldehyde with 3-chlorobenzohydrazide, 2-chlorobenzohydrazide, 4-nitrobenzohydrazide, and 3-nitrobenzohydrazide, respectively in 1:1 molar ratio in MeOH. X-ray diffraction quality single crystals were obtained by slow evaporation method. All the compounds are soluble in MeOH, EtOH, MeCN, DMF and DMSO.

3. 2. Structure Description of the Compounds

The molecular structures of the hydrazones **1**–**4** are shown in Figs. 1–4, respectively. Selected bond lengths and angles are listed in Table 2. Compound **1** contains one hydrazone molecule and a water molecule of crystallization.

Table 1. Crystallographic and experimental data for the compounds.

Compound	1	2	3	4
Formula	$C_{14}H_{12}ClFN_2O_2$	$C_{14}H_{10}ClFN_2O$	$C_{14}H_{10}FN_3O_3$	$C_{14}H_{10}FN_3O_3$
M_r	294.71	276.69	287.25	287.25
T (K)	298(2)	298(2)	298(2)	298(2)
Crystal system	Monoclinic	Triclinic	Monoclinic	Orthorhombic
Space group	$P2_1/n$	P-1	$P2_1/c$	$Pbca$
a (Å)	4.7433(8)	5.0121(11)	13.8257(15)	14.9204(13)
b (Å)	12.7365(12)	10.8580(13)	12.6853(13)	15.1431(13)
c (Å)	23.1503(15)	12.3750(13)	7.6638(11)	23.7602(15)
α (°)	90	97.413(1)	90	90
β (°)	94.576(1)	93.367(1)	101.447(1)	90
γ (°)	90	96.951(1)	90	90
V (Å^3)	1394.1(3)	661.03(18)	1317.4(3)	5368.4(7)
Z	4	2	4	16
D_c (g cm^{-3})	1.404	1.390	1.448	1.422
μ(Mo-Ka) (mm^{-1})	0.288	0.293	0.114	0.112
F(000)	608	284	592	2368
Reflections collected	5057	3475	5358	49187
Unique reflections	1658	2427	1790	4816
Observed reflections [$I \geq 2\sigma(I)$]	1291	1979	1411	2517
Parameters	190	175	193	385
Restraints	4	1	1	2
GooF on F^2	1.031	1.048	1.039	1.050
R_1, wR_2 [$I \geq 2\sigma(I)$][a]	0.0360, 0.0803	0.0421, 0.1097	0.0339, 0.0813	0.0508, 0.0863
R_1, wR_2 (all data)[a]	0.0515, 0.0878	0.0519, 0.1179	0.0476, 0.0892	0.1397, 0.1122
$\Delta\rho_{max}/\Delta\rho_{min}$, (eÅ^{-3})	0.214, –0.227	0.246, –0.286	0.133, –0.150	0.150, –0.190

[a] $R_1 = F_o - F_c/F_o$, $wR_2 = [\sum w(F_o^2 - Fc^2)/\sum w(F_o^2)^2]^{1/2}$

Compound **4** contains two independent hydrazone molecules. All the hydrazone molecules of the compounds adopt *E* configuration with respect to the methylidene units. The distances of the methylidene bonds, ranging from 1.26 to 1.28 Å, confirm them as typical double bonds. The shorter distances of the C–N bonds and the longer distances of the C=O bonds for the –C(O)–NH– units than usual, suggest the presence of conjugation effects in the molecules. All bond lengths in the compounds are comparable to each other, and within normal values.[20] The dihedral angles formed by the two benzene rings of the hydrazone molecules are 9.9(4)° for **1**, 8.1(5)° for **2**, 75.0(5)° for **3**, and 26.8(4)° and 19.3(4)° for **4**.

The hydrogen bonds information is summarized in Table 3. In the crystal structure of compound **1**, the hydrazone and water molecules are linked through O–H···O, N–H···O and C–H···O hydrogen bonds, to form two-dimensional sheets parallel to the *ab* plane. The sheets are further linked through C–H···F hydrogen bonds along the *c* axis, to form three-dimensional network (Fig. 5). In the crystal structure of compound **2**, the hydrazone molecules are linked through N–H···O and C–H···O hydrogen bonds, to form one-dimensional chains running along the *a* axis (Fig. 6). In the crystal structure of compound **3**, the hydrazone molecules are linked through N–H···O hydrogen bonds, to form one-dimensional chains along the *c* axis. The chains are further linked by C–H···F hydrogen bonds, to form two-dimensional sheets parallel to the *ac* plane (Fig. 7). In the crystal structure of compound **4**, the hydrazone molecules are linked through N–H···O, C–H···O and C–H···F hydrogen bonds, to form two-dimensional sheets parallel to the *ac* plane (Fig. 8). In addition, the weak π···π interactions among the benzene rings with centroid to centroid distances of 3.6–4.0 Å are observed in **3** and **4** (Table 4).

Table 2. Selected bond lengths (Å) and angles (°) for the compounds.

	1	**2**	**3**	**4**
C7–N1	1.275(3)	1.272(2)	1.273(2)	1.271(4)
N1–N2	1.381(3)	1.382(2)	1.391(2)	1.382(4)
N2–C8	1.340(3)	1.348(2)	1.343(2)	1.345(4)
C8–O1	1.235(3)	1.219(2)	1.234(2)	1.234(4)
C22–N4				1.275(4)
N4–N5				1.386(3)
N5–C23				1.343(4)
C23–O4				1.231(4)
C7–N1–N2	115.6(2)	115.5(2)	114.1(2)	115.8(2)
N1–N2–C8	118.5(2)	120.2(2)	120.3(2)	117.9(2)
N2–C8–C9	117.4(2)	114.1(2)	113.5(2)	117.1(2)
N2–C8–O1	122.1(2)	123.0(2)	124.1(2)	122.7(2)
C22–N4–N5				114.6(3)
N4–N5–C23				118.8(3)
N5–C23–C24				116.6(3)
N5–C23–O4				122.6(3)

Table 3. Hydrogen bond distances (Å) and bond angles (°) for the compounds.

D*–H···*A	***d*(*D*–H)**	***d*(H··*A*)**	***d*(*D*···*A*)**	**Angle (*D*–H···*A*)**
1				
O2–H2B···O1$^{\#1}$	0.85(1)	1.95(1)	2.800(3)	174(3)
O2–H2A···O1$^{\#2}$	0.85(1)	2.00(1)	2.817(3)	162(3)
N2–H2···O2$^{\#3}$	0.90(1)	1.98(1)	2.865(3)	168(3)
C12–H12···F1$^{\#4}$	0.93	2.51(2)	3.441(3)	176(3)
2				
N2–H2A···O1$^{\#5}$	0.89(1)	2.04(2)	2.862(2)	153(2)
C7–H7···O1$^{\#5}$	0.93	2.52(2)	3.194(3)	130(3)
3				
N2–H2···O1$^{\#6}$	0.90(1)	1.99(1)	2.871(2)	165(2)
C11–H11···F1$^{\#7}$	0.93	2.50(2)	3.275(3)	141(3)
4				
N2–H2···O4$^{\#8}$	0.90(1)	2.13(2)	2.970(3)	154(2)
N5–H5···O1$^{\#9}$	0.90(1)	2.06(1)	2.953(3)	172(3)
C5–H5A···F2$^{\#10}$	0.93	2.38(2)	3.276(3)	161(3)
C10–H10···O4$^{\#8}$	0.93	2.49(2)	3.400(3)	165(3)

Symmetry codes: #1: 1 + *x*, –1 + *y*, *z*; #2: *x*, –1 + *y*, *z*; #3: – *x*, – *y*, 1 – *z*; #4: 5/2 + *x*, ½ – *y*, ½ + *z*; #5: –1 + *x*, *y*, *z*; #6: *x*, ½ – *y*, ½ + *z*; #7: 1 + *x*, ½ – *y*, ½ + *z*; #8: –½ + *x*, *y*, ½ – *z*; #9: *x*, ½ – *y*, ½ + *z*; #10: 1 – *x*, – *y*, 1 – *z*.

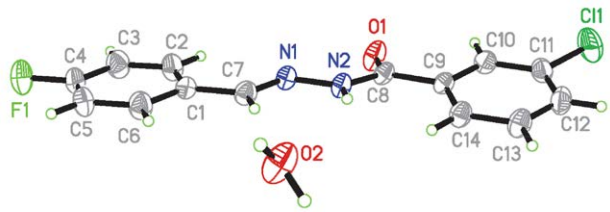

Fig. 1. A perspective view of the molecular structure of **1** with the atom labeling scheme. Thermal ellipsoids are drawn at the 30% probability level.

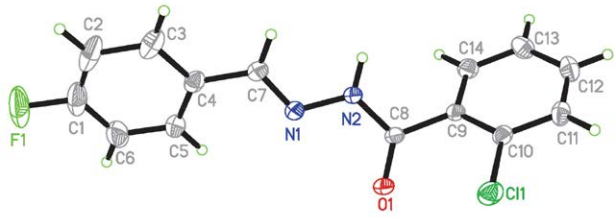

Fig. 2. A perspective view of the molecular structure of **2** with the atom labeling scheme. Thermal ellipsoids are drawn at the 30% probability level.

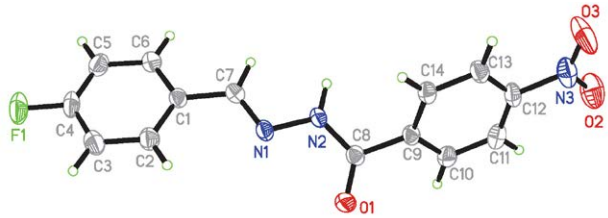

Fig. 3. A perspective view of the molecular structure of **3** with the atom labeling scheme. Thermal ellipsoids are drawn at the 30% probability level.

Table 4. Parameters between the planes for compounds **3** and **4**.

Cg	Distance between ring centroids (Å)	Dihedral angle (°)	Perpendicular distance of *Cg*(I) on *Cg*(J) (Å)	Beta angle (°)	Gamma angle (°)	Perpendicular distance of *Cg*(J) on *Cg*(I) (Å)
3						
*Cg*1–*Cg*1$^{\#11}$	3.6099	0	–3.3962	19.81	19.81	–3.3962
*Cg*2–*Cg*2$^{\#12}$	3.9006	0	–3.5234	25.41	25.41	–3.5234
4						
*Cg*3–*Cg*4$^{\#13}$	3.9169	19.287	–3.4087	10.85	29.51	–3.8469
*Cg*3–*Cg*5$^{\#14}$	3.7954	5.865	–3.4527	25.86	24.54	3.4155
*Cg*4–*Cg*3$^{\#15}$	3.9169	19.287	–3.8469	29.51	10.85	–3.4087
*Cg*4–*Cg*4$^{\#16}$	3.9285	0	3.4687	28.00	28.00	3.4687
*Cg*5–*Cg*3$^{\#14}$	3.7954	5.865	3.4155	24.54	25.86	3.4155

Cg1 and Cg2 are the centroids of C1-C2-C3-C4-C5-C6 and C9-C10-C11-C12-C13-C14 in 3, respectively. Cg3, Cg4 and Cg5 are the centroids of C1-C2-C3-C4-C5-C6, C9-C10-C11-C12-C13-C14 and C24-C25-C26-C27-C28-C29 in 4, respectively. Symmetry codes: #11: – *x*, 1 – *y*, – *z*; #12: 1 – *x*, – *y*, 1 – *z*; #13: ½ + *x*, ½ – *y*, – *z*; #14: *x*, *y*, *z*; #15: –½ + *x*, ½ – *y*, – *z*; #16: – *x*, 1 – *y*, – *z*.

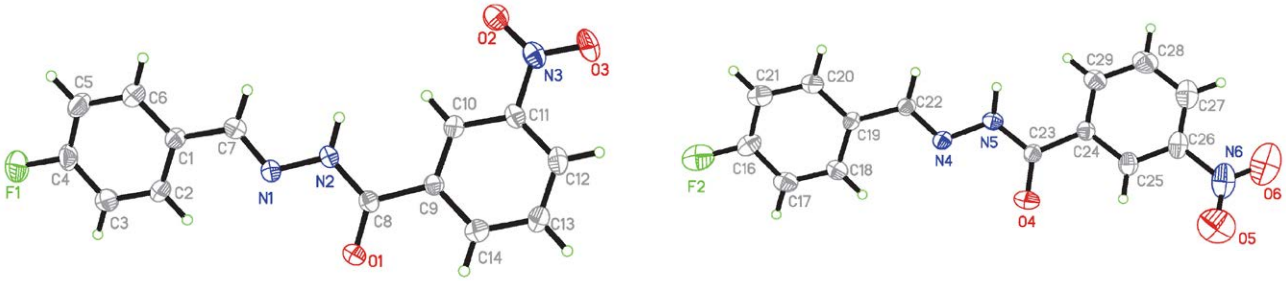

Fig. 4. A perspective view of the molecular structure of **4** with the atom labeling scheme. Thermal ellipsoids are drawn at the 30% probability level.

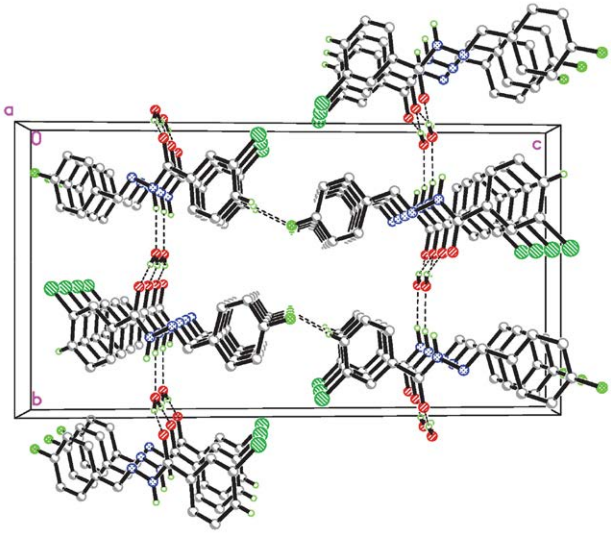

Fig. 5. The packing diagram of **1**. Dashed lines represent O–H···O, N–H···O and C–H···F interactions. C: silver; H: the smallest green; F: middle green; Cl: the largest green; N: blue; O: red.

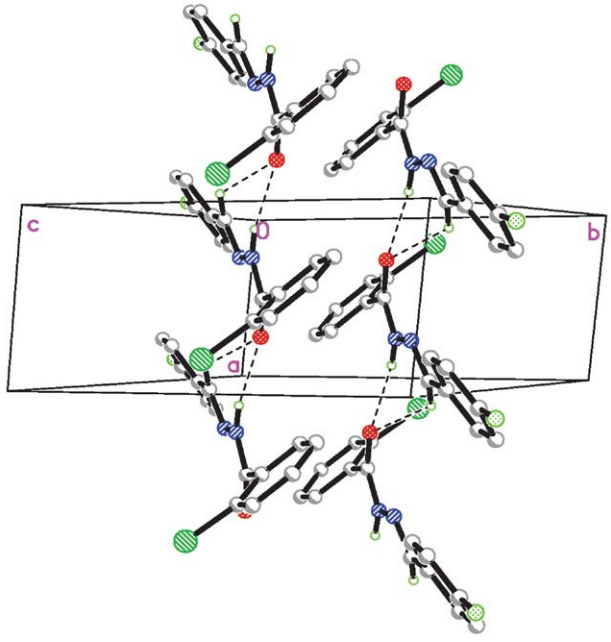

Fig. 6. The packing diagram of **2**. Dashed lines represent N–H···O and C–H···O interactions. C: silver; H: the smallest green; F: middle green; Cl: the largest green; N: blue; O: red.

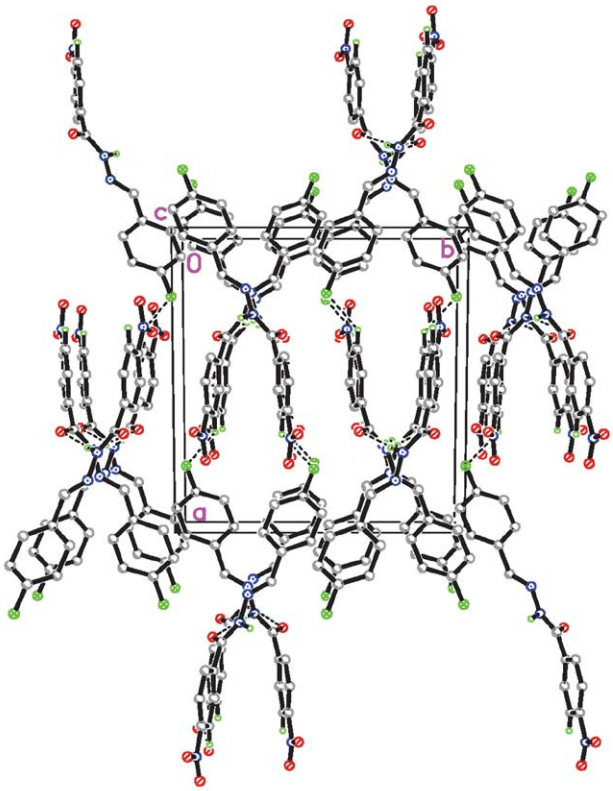

Fig. 7. The packing diagram of **3**. Dashed lines represent N–H···O and C–H···F interactions. C: silver; H: the smallest green; F: the largest green; N: blue; O: red.

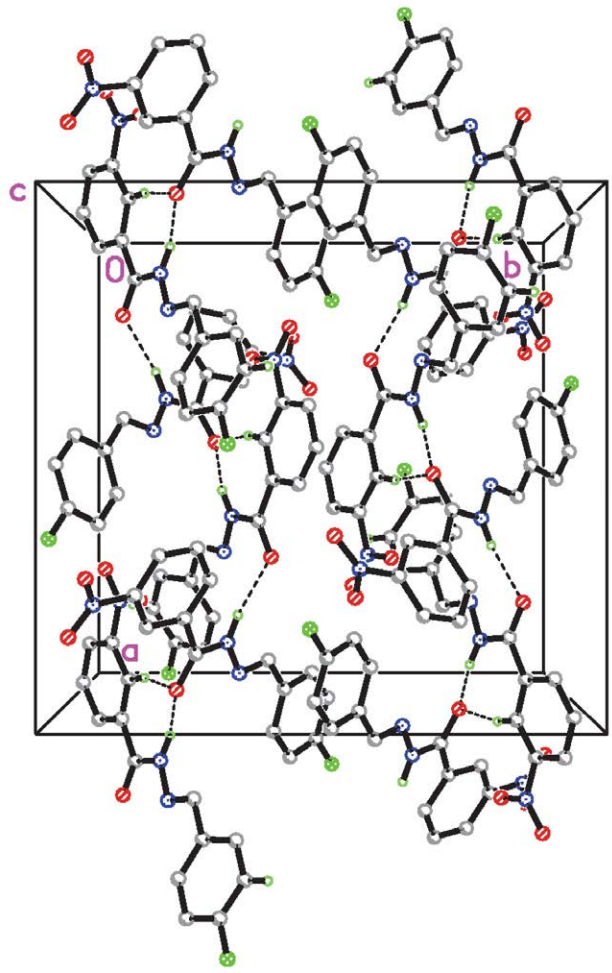

Fig. 8. The packing diagram of **4**. Dashed lines represent N–H···O, C–H···O and C–H···F interactions. C: silver; H: the smallest green; F: the largest green; N: blue; O: red.

3. 4. IR and ^{1}H NMR Spectra

In the IR spectra of the compounds, the weak and sharp bands at 3217 cm^{-1} (**1**), 3235 cm^{-1} (**2**), 3226 cm^{-1} (**3**) and 3227 cm^{-1} (**4**) are due to the N–H stretching vibrations. The compounds exhibit intense absorptions at 1649–1666 cm^{-1}, which can be attributed to the C=O vibrations. The strong absorptions at 1600–1608 cm^{-1} can be attributed to the C=N vibrations.[21] The bands indicative of the $\nu_{as}(NO_2)$ and $\nu_s(NO_2)$ vibrations are observed at 1522 and 1345 cm^{-1} for **1**, and 1532 and 1350 cm^{-1} for **2**.[21]

In the ^{1}H NMR spectra of the compounds, the absence of NH_2 signals and the appearance of peaks for NH protons in the region δ = 11.96–12.20 ppm and imine CH protons in the region δ = 8.30–8.51 ppm confirms the synthesis of the hydrazones. The aromatic proton signals were found in their respective regions with different multiplicities, confirming their relevant substitution pattern.

3. 5. Pharmacology

The assay of xanthine oxidase inhibition was performed for three parallel times. The results are given in Table 5. Allopurinol is a commercial xanthine oxidase inhibitor, which was used as a control drug. The percent of inhibition for the drug is 81.3 ± 2.8% at the concentration of 100 μmol L^{-1}, and the IC_{50} value is 8.5 ± 2.1 μmol L^{-1}. Compounds **1** and **2** have similar activities, with the percent of inhibition in the range of 67–73% and with IC_{50} value of 14–16 μmol L^{-1}. Compounds **3** and **4** also have similar activities, with the percent of inhibition in the range of 85–90% and with IC_{50} value of 6–7 μmol L^{-1}. Compounds **3** and **4** have better activities than allopurinol. The merely difference between compounds **1**, **2** and **3**, **4** are the Cl and NO_2 substituent groups. Thus, it is not difficult to conclude that NO_2 group contributes to the inhibition. This agrees well with our previously reported paper that NO_2 is a preferred group for the inhibition process.[15b] These findings are also coherent with the results reported in the literature that the existence of electron-withdrawing groups in the benzene rings can enhance the activities.[22]

Table 5. Inhibition of xanthine oxidase by the assayed compounds.

Tested materials	Percent of Inhibition[a]	IC_{50} (μmol L^{-1})
1	67.5 ± 2.6	15.2 ± 1.3
2	72.3 ± 2.5	14.3 ± 1.7
3	89.7 ± 2.3	6.1 ± 1.5
4	85.6 ± 3.0	6.3 ± 1.6
Allopurinol	81.3 ± 2.8	8.5 ± 2.1

[a] The concentration of the tested material is 100 μmol L^{-1}.

3. 6. Molecular Docking Study

Molecular docking technique was carried out to study the binding mode between the compounds and the active sites of xanthine oxidase (1FIQ in the Protein Data Bank). Allopurinol was used to verify the model of docking, with docking score of –6.27. Figs. 9-12 are the binding model for the four compounds, which show that the compounds can enter into the active pocket of the enzyme. The docking scores are –8.04 (**1**), –8.09 (**2**), –9.02 (**3**), and –9.21 (**4**), which are lower than allopurinol. The molecules of **1** and **2** bind with the enzyme through N–H···N hydrogen bonds with ALA1079. The molecules of **3** and **4** bind with the enzyme through N–H···O hydrogen bonds with ARG880 and THR1010.

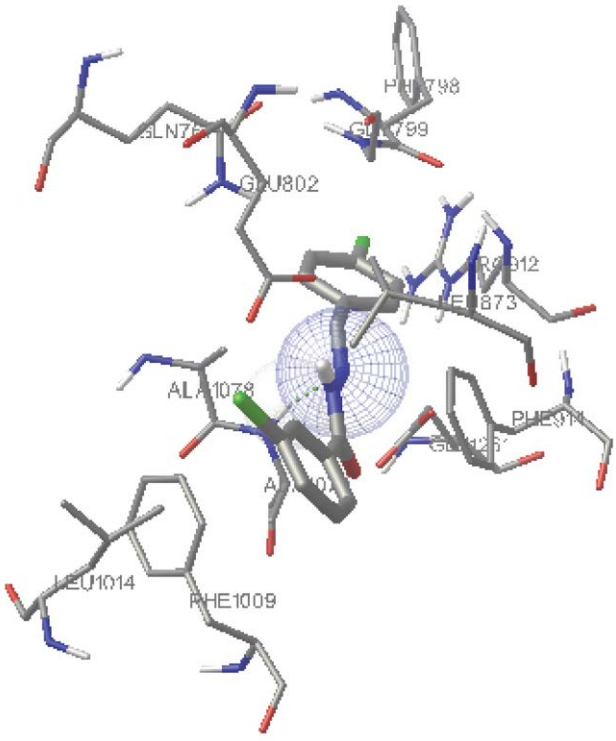

Fig. 9. 2D binding mode of **1** with the active site of xanthine oxidase. Dashed lines represent N–H···N interactions.

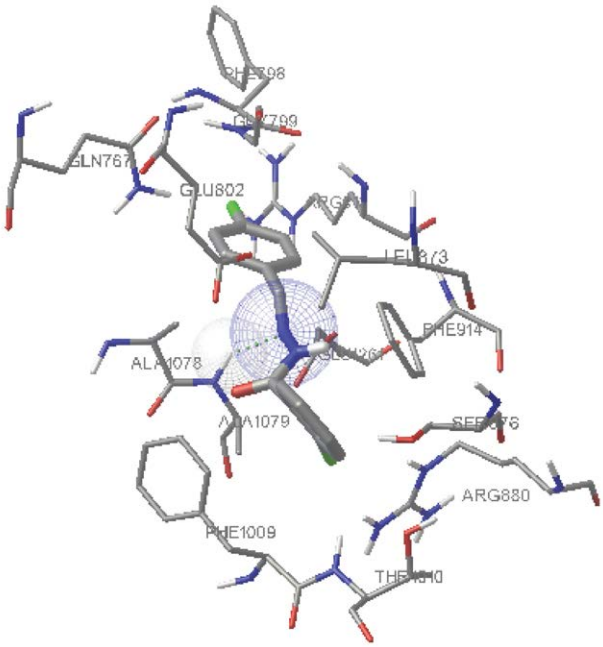

Fig. 10. 2D binding mode of **2** with the active site of xanthine oxidase. Dashed lines represent N–H···N interactions.

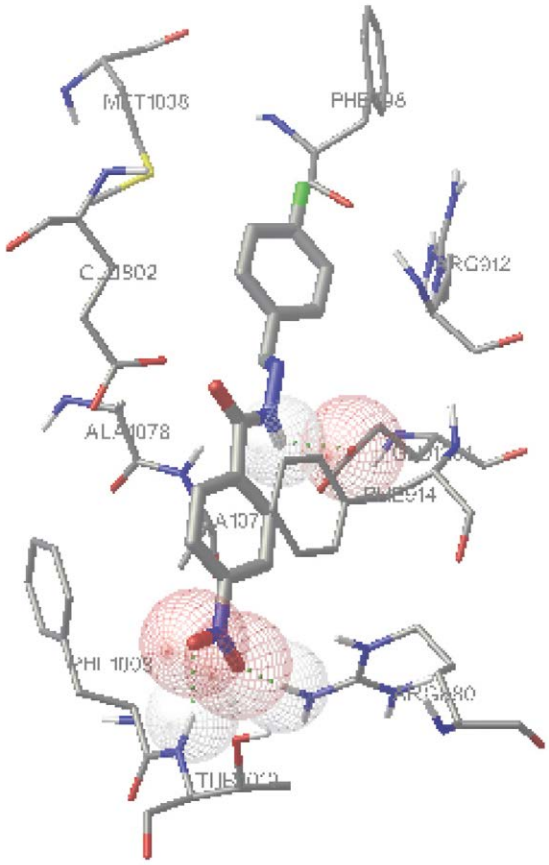

Fig. 11. 2D binding mode of **3** with the active site of xanthine oxidase. Dashed lines represent N–H···O interactions.

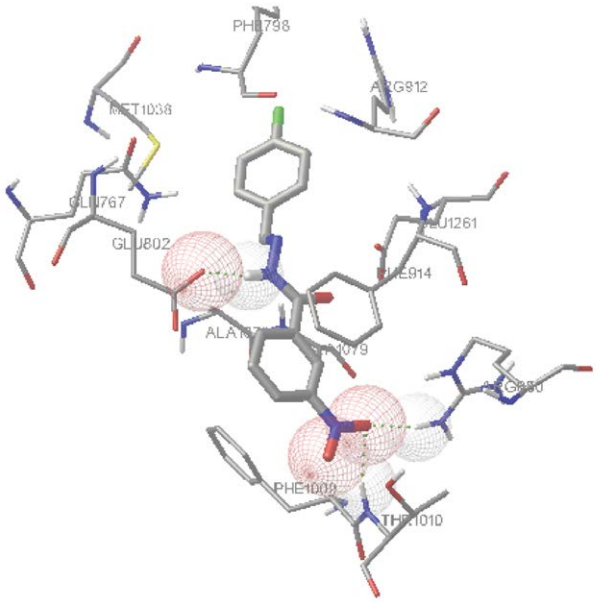

Fig. 12. 2D binding mode of **4** with the active site of xanthine oxidase. Dashed lines represent N–H···O interactions.

4. Conclusion

The present work reports the synthesis, X-ray crystal structures and xanthine oxidase inhibitory activity of four hydrazones. The compounds were characterized by CHN elemental analysis, infrared and ^{1}H NMR spectra, and single crystal X-ray determination. Among the compounds, those containing nitro groups have effective xanthine oxidase inhibitory activities with IC_{50} values of 6-7 μmol L^{-1}, which may be used as potential xanthine oxidase inhibitors. The molecules of the compounds filled well with the active pocket of the enzyme by hydrogen bonds.

Acknowledgments

This research was supported by the Henan Provincial Natural Science Foundation (No. 232300420103).

Supplementary Material

CCDC – 2286909 for **1**, 2286910 for **2**, 2286911 for **3**, and 2286912 for **4** contain the supplementary crystallographic data for this article. These data can be obtained free of charge at http://www.ccdc.cam.ac.uk/const/retrieving.html or from the Cambridge Crystallographic Data Centre (CCDC), 12 Union Road, Cambridge CB2 1EZ, UK; fax: +44(0)1223-336033 or e-mail: deposit@ccdc.cam.ac.uk.

5. References

1. (a) L. Tiano, R. Belardinelli, P. Carnevali, F. Principi, G. Seddaiu, G. P. Littarru, *Eur. Heart J.* **2007**, *28*, 2249–2255; **DOI:**10.1093/eurheartj/ehm267
(b) A. Pinto, M. Kornfeld, H. Aubin, P. Akhyari, A. Lichtenberg, *Free Rad. Biol. Med.* **2014**, *76*, S52–S52; **DOI:**10.1016/j.freeradbiomed.2014.10.420
(c) P. H. Chan, J. W. Schimidley, R. A. Fishman, S. M. Longar, *Neurology* **1984**, *34*, 315–320. **DOI:**10.1212/WNL.34.3.315
2. (a) A. A. Fatokun, T. W. Stone, R. A. Smith, *Neurosci. Lett.* **2007**, *416*, 34–38; **DOI:**10.1016/j.neulet.2007.01.078
(b) X. Yu, L. Zhang, P. Zhang, J. Zhi, R. N. Xing, L. Q. He, *Pharm. Biol.* **2020**, *58*, 944–949; **DOI:**10.1080/13880209.2020.1817951
(c) E. O. Dangana, T. E. Omolekulo, E. D. Areola, K. S. Olaniyi, A. O. Soladoye, L. A. Olatunji, *Chem. Biol. Interact.* **2020**, *316*, 108929; **DOI:**10.1016/j.cbi.2019.108929
(d) J. Nomura, N. Busso, A. Ives, C. Matsui, S. Tsujimoto, T. Shirakura, M. Tamura, T. Kobayashi, A. So, Y. Yamanaka, *Sci. Rep.* **2014**, *4*, 4554; **DOI:**10.1038/srep04554
(e) B. Butts, D. A. Calhoun, T. S. Denney, S. G. Lloyd, H. Gupta, K. K. Gaddam, I. Aban, S. Oparil, P. W. Sanders, R. Patel, J. F. Collawn, L. J. Dellitalia, *Free Rad. Biol. Med.* **2019**, *134*, 343–349; **DOI:**10.1016/j.freeradbiomed.2019.01.029
(f) P. Pacher, A. Nivorozhkin, C. Szabo, *Pharmacol. Rev.* **2006**, *58*, 87–114. **DOI:**10.1124/pr.58.1.6
3. (a) C. A. Hay, J. A. Prior, J. Belcher, C. D. Mallen, E. Roddy, *Arthr. Care Res.* **2021**, *73*, 1049–1054; **DOI:**10.1002/acr.24205
(b) P. C. Robinson, N. Dalbeth, P. Donovan, *Arthr. Care Res.* **2021**, *73*, 1537–1543; **DOI:**10.1002/acr.24357
(c) S. Z. Zhang, T. Xu, Q. Y. Shi, S. Y. Li, L. Wang, Z. M. An, N. Su, *Front. Med.* **2021**, *8*, 698437; **DOI:**10.3389/fmed.2021.698437
(d) A. Jeyaruban, W. Hoy, A. Cameron, H. Healy, Z. Wang, J. Zhang, A. Mallett, *J. Nephrol.* **2021**, *34*, 753–762; **DOI:**10.1007/s40620-020-00937-4
(e) L. G. Gao, B. Wang, Y. Pan, Y. Lu, R. Cheng, *Clin. Cardiol.* **2021**, *44*, 907–916. **DOI:**10.1002/clc.23643
4. (a) G. Beyer, M. F. Melzig, *Biol. Pharm. Bull.* **2005**, *28*, 1183–1186; **DOI:**10.1248/bpb.28.1183
(b) A. Smelcerovic, K. Tomovic, Z. Smelcerovic, Z. Petronijevic, G. Kocic, T. Tomasic, Z. Jakopin, M. Anderluh, *Eur. J. Med. Chem.* **2007**, *135*, 491–516.
5. (a) J. X. Zhao, Q. Mao, F. W. Lin, B. Zhang, M. Sun, T. J. Zhang, S. J. Wang, *Eur. J. Med. Chem.* **2022**, *229*, 114086;
(b) N. Zhai, C. C. Wang, F. S. Wu, L. W. Xiong, X. G. Luo, X. L. Ju, G. Y. Liu, *Inter. J. Mol. Sci.* **2021**, *22*, 8122. **DOI:**10.3390/ijms22158122
6. (a) T.-J. Zhang, S. Tu, X. Zhang, Q.-Y. Wang, S.-S. Hu, Y. Zhang, Z.-H. Zhang, Z.-R. Wang, F.-H. Meng, *Bioorg. Chem.* **2021**, *117*, 105417; **DOI:**10.1016/j.bioorg.2021.105417
(b) B. Zhang, Y. L. Duan, Y. W. Yang, Q. Mao, F. W. Lin, J. Gao, X. W. Dai, P. Zhang, Q. H. Li, J. X. Li, R. H. Dai, S. J. Wang, *Eur. J. Med. Chem.* **2022**, *227*, 113928.
7. H. Hayun, R. Hanifati, A. D. Pratiwik, *Indian J. Pharm. Sci.* **2021**, *83*, 1074–1080.
8. S. Tu, T.-J. Zhang, Y. Zhang, X. Zhang, Z.-H. Zhang, F.-H. Meng, *Bioorg. Chem.* **2021**, *115*, 105181.

9. A. Alsayari, M. Z. Hassan, Y. I. Asiri, A. Bin Muhsinah, M. Kamal, M. S. Akhtar, *Indian J. Heterocycl. Chem.* **2021**, *31*, 635–640.
10. J. L. Serrano, D. Lopes, M. J. A. Reis, R. E. F. Boto, S. Silvestre, P. Almeida, *Biomedicines* **2021**, *9*, 1443. **DOI:**10.3390/biomedicines9101443
11. (a) G.-X. He, L.-W. Xue, Q.-L. Peng, P.-P. Wang, H.-J. Zhang, *Acta Chim. Slov.* **2019**, *66*, 570–575; **DOI:**10.17344/acsi.2018.4868
(b) C.-L. Zhang, X.-Y. Qiu, S.-J. Liu, *Acta Chim. Slov.* **2019**, *66*, 484–489; **DOI:**10.17344/acsi.2019.5019
(c) J. Qin, Q. Yin, S.-S. Zhao, J.-Z. Wang, S.-S. Qian, *Acta Chim. Slov.* **2016**, *53*, 55–61; **DOI:**10.17344/acsi.2015.1918
(d) F. Qureshi, M. Y. Khuhawar, T. M. Jahangir, A. H. Channar, *Acta Chim. Slov.* **2016**, *63*, 113–120; **DOI:**10.17344/acsi.2015.1994
(e) X.-Q. Luo, Q.-R. Liu, Y.-J. Han, L.-W. Xue, *Acta Chim. Slov.* **2020**, *67*, 159–166; **DOI:**10.17344/acsi.2019.5303
(f) K. M. El-Mahdy, A. M. E.-Kazak, M. Abdel-Megid, M. Seada, O. Farouk, *Acta Chim. Slov.* **2016**, *67*, 18–25; **DOI:**10.17344/acsi.2015.1555
(g) M. Kaur, S. Kumar, M. Yusuf, J. Lee, R. J. C. Brown, K. H. Kim, A. K. Malik, *Coord. Chem. Rev.* **2021**, *449*, 214214. **DOI:**10.1016/j.ccr.2021.214214
12. (a) N. Choudhary, D. L. Hughes, U. Kleinkes, L. F. Larkworthy, G. J. Leigh, M. Maiwald, C. J. Marmion, J. R. Sanders, G. W. Smith, C. Sudbrake, *Polyhedron* **1997**, *16*, 1517–1528; **DOI:**10.1016/S0277-5387(96)00436-6
(b) M. Leigh, C. E. Castillo, D. J. Raines, A. K. Duhme-Klair, *ChemMedChem* **2011**, *6*, 612–616. **DOI:**10.1002/cmdc.201000429
13. (a) S. Rollas, S.G. Kucukguzel, *Molecules* **2007**, *12*, 1910–1939; **DOI:**10.3390/12081910
(b) S. Omidi, A. Kakanejadifard, *RSC Adv.* **2020**, *10*, 30186–30202; **DOI:**10.1039/D0RA05720G
(c) D. Blanot, J. Lee, S.E. Girardin, *Chem. Biol. Drug Des.* **2012**, *79*, 2–8; **DOI:**10.1111/j.1747-0285.2011.01204.x
(d) Z.A. Kaplancikli, M.D. Altintop, A. Ozdemir, G. Turan-Zitouni, S.I. Khan, N. Tabanca, *Lett. Drug Des. Discov.* **2012**, *9*, 310–315; **DOI:**10.2174/157018012799129828
(e) K. Akdag, F. Tok, S. Karakus, O. Erdogan, O. Cevik, B. Kocyigit-Kaymakcioglu, *Acta Chim. Slov.* **2022**, *69*, 863–875; **DOI:**10.17344/acsi.2022.7614
(f) G.-X. He, L.-W. Xue, *Acta Chim. Slov.* **2021**, *68*, 567–574. **DOI:**10.17344/acsi.2020.6333
14. (a) L. C. Felton, J.H. Brewer, *Science* **1947**, *105*, 409–410; **DOI:**10.1126/science.105.2729.409
(b) M. Gopalakrishnan, J. Thanusu, V. Kanagarajan, R. Govindaraju, *J. Enzym. Inhib. Med. Ch.* **2009**, *24*, 52–58; **DOI:**10.1080/14756360801906632
(c) L. Shi, H.-M. Ge, S.-H. Tan, H.-Q. Li, Y.-C. Song, H.-L. Zhu, R.-X. Tan, *Eur. J. Med. Chem.* **2007**, *42*, 558–564. **DOI:**10.1016/j.ejmech.2006.11.010
15. (a) L.-W. Xue, S.-T. Li, Y.-J. Han, X.-Q. Luo, *Acta Chim. Slov.* **2022**, *69*, 385–392; **DOI:**10.17344/acsi.2021.7252
(b) Y.-J. Han, X.-Y. Guo, L.-W. Xue, *Acta Chim. Slov.* **2022**, *69*, 928–936. **DOI:**10.17344/acsi.2022.7817
16. L. D. Kong, Y. Zhang, X. Pan, R. X. Tan, C. H. K. Cheng, Cell Mol. *Life Sci.* **2000**, *57*, 500–505. **DOI:**10.1007/PL00000710
17. Bruker, SMART and SAINT. Bruker AXS Inc., Madison, Wisconsin, USA (2002).
18. G. M. Sheldrick, SADABS. Program for Empirical Absorption Correction of Area Detector, University of Göttingen, Germany (1996).
19. G. M. Sheldrick, *Acta Crystallogr.* **2008**, *A64*, 112–122. **DOI:**10.1107/S0108767307043930
20. (a) F. H. Allen, O. Kennard, D. G. Watson, L. Brammer, A.G. Orpen, R. Taylor, *J. Chem. Soc. Perkin Trans. 2*, S1, (1987);
(b) L.-W. Xue, S.-T. Li, Y.-J. Han, X.-Q. Luo, *Acta Chim. Slov.* **2022**, *69*, 385–392; **DOI:**10.17344/acsi.2021.7252
(c) F.-M. Wang, L.-J. Li, G.-W. Zang, T.-T. Deng, Z.-L. You, *Acta Chim. Slov.* **2021**, *68*, 541–547; **DOI:**10.17344/acsi.2020.6051
(d) H.-Y. Zhu, *Acta Chim. Slov.* **2021**, *68*, 65–71;
(e) C.R. Bhimapaka, N.R. Rayala, R. Kommera, D. Cherupally, R.M. Thampunuri, V.K. Shasi, *Acta Chim. Slov.* **2018**, *65*, 34–49. **DOI:**10.17344/acsi.2017.3453
21. M. Zhang, D.-M. Xian, H.-H. Li, J.-C. Zhang, Z.-L. You, *Aust. J. Chem.* **2012**, *65*, 343–350. **DOI:**10.1071/CH11424
22. S. Gupta, L.M. Rodrigues, A.P. Esteves, A.M.F. Oliveira-Campos, M.S.J. Nascimento, N. Nazareth, H. Cidade, M.P. Neves, E. Fernandes, M. Pinto, N.M.F.S.A. Cerqueira, N. Bras, *Eur. J. Med. Chem.* **2008**, *43*, 771–780. **DOI:**10.1016/j.ejmech.2007.06.002

Povzetek

Štiri nove fluor vsebujoče hidrazone smo sintetizirali iz 4-fluorobenzaldehida s kloro- in nitro-substituiranimi benzohidrazidi. To so 3-kloro-*N*'-(4-fluorobenziliden)benzohidrazid (**1**), 2-kloro-*N*'-(4-fluorobenziliden)benzohidrazid (**2**), *N*'-(4-fluorobenziliden)-4-nitrobenzohidrazid (**3**) in ***N***'-(4-fluorobenziliden)-3-nitrobenzohidrazid (**4**). Spojine smo okarakterizirali z IR in ^{1}H NMR spektroskopijo ter z rentgenskih monokristalno strukturno analizo. Inhibitorna aktivnost ksantin oksidaze (XO) je pokazala, da sta nitro-substituirani spojini **3** in **4** aktivni. Izvedli smo docking simulacijo z vstavitvijo molekul spojin v aktivno mesto v kristalni strukturi ksantin oksidaze, da bi raziskali možne načine vezave.